# **Inorganic Chemistry**

pubs.acs.org/IC Featured Article

# A Macrocyclic Ligand Framework That Improves Both the Stability and $T_1$ -Weighted MRI Response of Quinol-Containing $H_2O_2$ Sensors

Sana Karbalaei, Erik Knecht, Alicja Franke, Achim Zahl, Alexander C. Saunders, P. Raj Pokkuluri, Ronald J. Beyers, Ivana Ivanović-Burmazović, and Christian R. Goldsmith\*



Cite This: Inorg. Chem. 2021, 60, 8368-8379



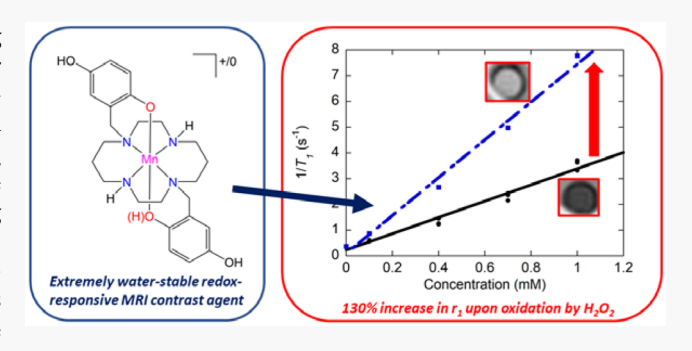
ACCESS

Metrics & More

Article Recommendations

s Supporting Information

**ABSTRACT:** Previously prepared Mn(II)- and quinol-containing magnetic resonance imaging (MRI) contrast agent sensors for  $H_2O_2$  relied on linear polydentate ligands to keep the redoxactivatable quinols in close proximity to the manganese. Although these provide positive  $T_1$ -weighted relaxivity responses to  $H_2O_2$  that result from oxidation of the quinol groups to p-quinones, these reactions weaken the binding affinity of the ligands, promoting dissociation of Mn(II) from the contrast agent in aqueous solution. Here, we report a new ligand, 1,8-bis(2,5-dihydroxybenzyl)-1,4,8,11-tetraazacyclotetradecane, that consists of two quinols covalently tethered to a cyclam macrocycle. The macrocycle provides stronger thermodynamic and kinetic barriers for metal-



ion dissociation in both the reduced and oxidized forms of the ligand. The Mn(II) complex reacts with  $H_2O_2$  to produce a more highly aquated Mn(II) species that exhibits a 130% greater  $r_1$ , quadrupling the percentile response of our next best sensor. With a large excess of  $H_2O_2$ , there is a noticeable induction period before quinol oxidation and  $r_1$  enhancement occurs. Further investigation reveals that, under such conditions, catalase activity initially outcompetes ligand oxidation, with the latter occurring only after most of the  $H_2O_2$  has been depleted.

# **■ INTRODUCTION**

The overproduction of reactive oxygen species (ROS), such as  $\rm H_2O_2$  and  $\rm O_2^-$ , has been implicated in a wide array of pathologies, including a host of neurological and cardiovascular health conditions. Given the possible roles of ROS in disease, our research group has strived to develop molecular probes that can be used to noninvasively monitor ROS concentrations in physiological environments. Such sensors could potentially distinguish pathologies with similar clinical symptoms and better inform preventative and ameliorative therapies. To this end, our laboratory has reported a series of complexes that respond to  $\rm H_2O_2$  with changes in their  $T_1$ -weighted relaxivity  $(r_1)$ .  $^{6-9}$ 

Recent sensors from our laboratory have consisted of Mn(II) ions complexed to quinol-containing polydentate ligands (Scheme 1). Positive  $r_1$  responses to  $H_2O_2$  are observed with  $N_4O_2$  or  $N_5O$  coordination spheres, where the nitrogen donors come from either neutral pyridine or amine groups. With a weakly anionic coordination sphere, the Mn(III/II) reduction potential is high enough to discourage oxidation of the metal to the less paramagnetic 3+ oxidation state. Terminal oxidants, such as  $H_2O_2$ , instead preferentially oxidize the ligand, differentiating our sensors from redoxresponsive magnetic resonance imaging (MRI) contrast agents reported by Gale, Caravan, and others.

quinol portions of the ligands to p-quinones is accompanied by an increase in  $r_1$ . Water molecules are proposed to displace p-quinones from the metal center, enhancing  $r_1$  through better aquation of Mn(II).<sup>8</sup> Having a second quinol in the coordination sphere generally improves the  $r_1$  response to  $H_2O_2$ . The relaxivities of  $[Mn(H_2qp1)(MeCN)]^{2+}$  (MeCN = acetonitrile) and  $[Mn(H_4qp2)Br_2]$  (3) increase by 10% and 30%, respectively, upon oxidation by excess  $H_2O_2$ .<sup>7,8</sup>

This strategy necessarily relies on a weakening of the ligand's affinity for Mn(II), and in the case of 3, a substantial portion of the metal ion is likely released upon oxidation by  $H_2O_2$ .<sup>8</sup> Anionic groups and macrocycles are frequently used to stabilize Gd(III)- and Mn(II)-containing MRI contrast agents.<sup>13,14</sup> We had previously replaced the  $H_4$ qp2 pyridines with carboxylic acids in order to stabilize the Mn(II) complexes; the carboxylic acids entirely deprotonate to carboxylates at pH 7. Although the more anionic  $H_3$ qc1<sup>3–</sup> and  $H_2$ qc1<sup>4–</sup> forms of the  $H_6$ qc1 ligand do indeed allow it to

Received: March 23, 2021 Published: May 27, 2021





Scheme 1. Molecular Structures of the Quinol-Containing Polydentate Ligands and Compositions of the Coordination Complexes Mentioned in This Paper

$$H_{2}$$
qp1  $H_{4}$ qp2  $H_{6}$ qc1  $H_{4}$ qp4

$$\begin{split} &[Mn^{II}(H_3qp4)](OTf) - 1 \\ &[Mn^{II}(H_2qp1)(MeCN)](OTf)_2 - 2 \\ &[Mn^{II}(H_4qp2)Br_2] - 3 \\ &[Mn^{III}(H_2qp4)](OTf) - 4 \end{split}$$

coordinate more tightly to the dicationic metal center, the additional negative charges in the coordination sphere render the manganese more susceptible to oxidation. Oxidation of the metal center to the less paramagnetic Mn(III) eliminates the  $r_1$  response of this complex to  $H_2O_2$ . A Mn(II) complex with a fluorinated tetradentate ligand with nearly identical chelating groups likewise gets readily oxidized to a lower-relaxivity Mn(III) species upon reaction with excess  $H_2O_2$ .

The other strategy to discourage metal release would be to incorporate a macrocycle into the ligand framework to stabilize the resultant transition-metal complexes both thermodynamically and kinetically. Here, we synthesize a new macrocyclic ligand, 1,8-bis(2,5-dihydroxybenzyl)-1,4,8,11-tetraazacyclotetradecane ( $H_4$ qp4), and its complex with Mn(II). We find that the redox reactivity of the Mn(II) compound is similar to those of the Mn(II) complexes with  $H_2$ qp1 and  $H_4$ qp2 in that (1) the reactivity with air is slight and (2) the reactivity with  $H_2$ O<sub>2</sub> primarily oxidizes the ligand rather than the metal ion. In addition to the anticipated stabilization of the Mn(II) complexes with the quinol and p-quinone forms of the ligand, inclusion of the macrocycle improves the maximal MRI response, with  $r_1$  increasing by 130% upon oxidation by  $H_2$ O<sub>2</sub>.

### EXPERIMENTAL SECTION

**Materials.** All chemicals and solvents were purchased from Sigma-Aldrich and used as received unless otherwise noted. All deuterated solvents were bought from Cambridge Isotopes. Diethyl ether and methanol (MeOH) were bought from Fisher. Methylene chloride  $(CH_2Cl_2)$  was purchased from Mallinckrodt Baker.

Instrumentation. All <sup>1</sup>H and <sup>13</sup>C NMR spectra were recorded on either a 400 MHz or a 600 mHz AV Bruker NMR spectrometer. All reported NMR resonance peak frequencies were referenced to internal standards. <sup>17</sup>O NMR data were collected on a Bruker AVANCE DRX 400WB spectrometer with a superconducting widebore magnet operating at a 54.24 MHz resonance frequency and a 9.4 T magnetic induction. A Varian Cary 50 spectrophotometer was used to collect optical data, which were then processed using software from the WinUV Analysis Suite. Electron paramagnetic resonance (EPR) spectra were collected using a Bruker EMX-6/1 X-band EPR spectrometer operated in the perpendicular mode and subsequently

analyzed with the program EasySpin. All EPR samples were run as frozen solutions in quartz tubes. We used a Johnson Matthey magnetic susceptibility balance (model MK I#7967) to measure the magnetic moments of solid samples of the metal complexes and estimated the diamagnetic component of the susceptibility using Pascal's constants.<sup>17</sup> Cyclic voltammetry (CV) was performed under N<sub>2</sub> at 294 K with an Epsilon electrochemistry workstation (Bioanalytical System, Inc.). The working, auxiliary, and reference electrodes were gold, platinum wire, and silver/silver(I) chloride, respectively. High-resolution mass spectrometry (HR-MS) data were collected at the Mass Spectrometer Center at Auburn University on a Bruker microflex LT matrix-assisted laser desorption ionization timeof-flight (MALDI-TOF) mass spectrometer via direct probe analysis operated in the positive-ion mode. Solid samples of the Mn(II) complex were dried, stored under N2, and sent to Atlantic Microlabs (Norcross, GA) for elemental analysis.

**X-ray Crystallography.** Crystallographic data for  $(H_6qp4)(OTf)_2$  and the oxidized product  $[Mn^{II}(H_2qp4)](OTf)$  were collected using a Bruker D8 VENTURE  $\kappa$ -geometry diffractometer system equipped with an Incoatec  $I\mu S$  3.0 microfocus sealed tube and a multilayer mirror monochromator (Mo  $K\alpha$ ,  $\lambda=0.71073$  Å). Diffraction data were integrated with the Bruker SAINT software package using a narrow-frame algorithm. Data were corrected for absorption effects using the Multiscan method (SADABS). The structure was solved and refined using the Bruker SHELXTL software package. Selected crystallographic data are presented in the Supporting Information and Table 1.

Potentiometric Titrations. The aqueous speciations of H<sub>4</sub>qp4 and its Mn(II) complex were assessed using a METROHM 765 Dosimat with a jacketed, airtight glass titration vessel. A Fisher Scientific Accumet Research AR15 pH meter was used to monitor the pH of the sample solutions during the titrations. The electrode was calibrated before each titration using commercially available standard solutions buffered to pH 4.0, 7.0, and 10.0. All samples were purged with argon prior to analysis and subsequently analyzed under an argon atmosphere at 25 °C to prevent carbonate contamination. All solution samples were prepared in solutions of 100 mM KCl in deionized Millipore water. The titrations investigating metal/ligand speciation were run with solutions that contained a 1:1 molar mixture of the ligand and MnCl<sub>2</sub>·4H<sub>2</sub>O. Carbonate-free solutions of 0.10 M KOH and 0.10 M HCl were prepared using argon-saturated deionized Millipore water. The titration data were analyzed and fit to speciation models using the Hyperquad2006 program.

Table 1. Selected Crystallographic Data for [H<sub>6</sub>qp4](OTf)<sub>2</sub> and 4

parameter	$[H_6qp4](OTf)_2$	$[Mn(H2qp4)](OTf)\cdot CH2Cl2$ (4)			
formula	$C_{26}H_{38}F_6N_4O_{10}S_2$	$C_{26}H_{35}Cl_2F_3MnN_4O_7S$			
MW	744.72	730.48			
cryst syst	triclinic	monoclinic			
space group	$P\overline{1}$	$P12_1/m1$			
a (Å)	9.2212(3)	8.3460(2)			
b (Å)	10.0950(4)	19.4089(5)			
c (Å)	10.4689(3)	9.9382(3)			
$\alpha$ (deg)	107.310(1)	90			
$\beta$ (deg)	111.234(1)	108.9230(10)			
γ (deg)	104.783(1)	90			
$V(Å^3)$	791.83(5)	1522.85(7)			
Z	1	2			
cryst color	colorless	pale red			
T (K)	110	110			
reflns collected	63351	36113			
unique reflns	5270	3586			
$R1(F) [I > 2\sigma(I)]^a$	0.0492	0.0259			
$wR2(F^2)$ (all data) <sup>a</sup>	0.1415	0.0837			
${}^{a}$ R1 = $\sum   F_{o}  -  F_{c}   / \sum  F_{o} $ ; wR2 = $[\sum w(F_{o}^{2} - F_{c}^{2})^{2} / \sum w(F_{o}^{2})^{2}]^{1/2}$ .					

High-Pressure Liquid Chromatography (HPLC). HPLC was performed with UV detection at 254 nm using an Agilent 1100 series apparatus and an Agilent Zorbax SB-C18 column (4.6 × 150 mm; 5  $\mu$ m pore size). The following eluents were used: (A) 99.9% water with 0.1% trifluoroacetic acid (TFA); (B) 99.9% MeCN with 0.1% TFA. The following method was used: gradient = 90% A and 10% B to 100% B over 20 min, flow rate = 0.20 mL/min, injection volume = 25.0  $\mu$ L, and column temperature = 37.0 °C. Before each run, the HPLC instrument was flushed with eluent 100% A to 100% B over 16 min with a flow rate of 0.49 mL/min and an injection volume of 25.0  $\mu$ L.

Measurement of the Aquation Numbers (a). The a values were calculated from the maximum <sup>17</sup>O transverse relaxivity,  $r_{2\text{max}}$ and the equation  $q = r_{2\text{max}}^{\circ}/510$ . Gale, Zhu, and Caravan previously used this relationship to estimate the inner-sphere hydration state of Mn(II) in coordination complexes. <sup>19</sup> Relaxation rates were measured both for aqueous solutions containing Mn(II) complexes and for metal-free solutions buffered to pH 7.4. The line widths at half-height of the signal were determined by a deconvolution procedure on the real part of the Fourier-transformed spectra with a Lorentzian shape function in the data analysis module of Bruker Topspin 1.3 software. The measurements were performed with a commercial 5 mm Bruker broadband probe thermostated with a Bruker B-VT 3000 variabletemperature unit. Samples were prepared by adding a solution of solid dissolved in a minimal amount of MeCN to an aqueous solution containing either 60 mM 4-(2-hydroxyethyl)-1-piperazineethanesulfonic acid (HEPES) or 60 mM 3-(N-morpholino)propanesulfonic acid (MOPS) buffered to pH 7.4. <sup>17</sup>O-labeled water (10%; D-Chem Ltd., Tel Aviv, Israel) was added to these solutions, resulting in a total enrichment of 1% <sup>17</sup>O in the studied samples. The resultant mixtures contained either 6.0 or 2.5 mM of the Mn(II) complex. The 2.5 mM sample was oxidized by 15 equiv of H2O2 for 15 min prior to data acquisition. The temperature dependence of the <sup>17</sup>O-line broadening was studied from 274.2 to 338.2 K.

**MRI.** All MRI data were collected at the Auburn University MRI Research Center on a Siemens Verio open-bore 3-T MRI clinical scanner. A 15-channel knee coil was used to simultaneously image 12–15 samples. The imaging procedure was identical with those used for similar studies from our laboratory. <sup>6–9,20</sup> An inversion—recovery (IR) sequence was used that featured a nonselective adiabatic inversion pulse followed by a slice-selective gradient-recalled-echo (GRE) readout after a delay period corresponding to the inversion time (TI). <sup>21,22</sup> The GRE was a saturation readout, such that only one

line of k space was acquired per repetition time (TR), in order to maximize both the signal strength and accuracy of the  $T_1$  estimates. The specific imaging parameters were as follows: TR was set to 10 s, TI was varied from 10 to 2600 ms over 20 steps, the echo time (TE) was set to 2.75 ms, the flip angle equaled 90°, averages = 1, slice thickness = 10 mm, field of view =  $64 \times 64$  mm, and matrix =  $64 \times 64$ , resulting in a pixel size of  $1.0 \times 1.0 \times 10.0$  mm. All samples were run in 50 mM solutions of HEPES in water, buffered to pH 7.0 and kept at 22 °C. The manganese content was systematically varied from 0.10 to 1.00 mM. The inverses of the  $T_1$  values from two separate batches of contrast agent were plotted versus the concentration of Mn(II) to obtain  $T_1$  values.

MRI Data Analysis. Image analysis was performed using custom Matlab programs (Mathworks, Natick, MA). The initial TI = 4.8 ms image was used as a baseline to determine circular region of interest (ROI) boundaries for each sample; from these, the mean pixel magnitudes for each ROI were calculated. For each of the 36 subsequent TI images, the same ROI boundaries were applied, and the mean pixel magnitude calculations were repeated. This gave consistent ROI spatial definitions and a corresponding time course of magnitudes for each of the samples over all of the TI time points. Each sample's complex phase was used to correct the magnitude polarity to produce a complete exponential  $T_1$  IR curve. The Nelder–Mead simplex algorithm  $^{2.5}$  was applied to each sample's exponential curve to estimate its corresponding  $T_1$  value.

Preliminary Analysis of the Catalase Activity. In order to assess the ability of the Mn(II) complex to catalyze the degradation of  $\rm H_2O_2$ , we reacted 100 nM 1 with 10 mM  $\rm H_2O_2$  in a 100 mM phosphate solution buffered to pH 7.0 and monitored the absorbance at 240 nm over time.  $\rm H_2O_2$  has a molar extinction coefficient of 39.4  $\rm M^{-1}$  cm<sup>-1</sup> at this wavelength. The consumption of  $\rm H_2O_2$  was evaluated using a Shimadzu UV-1601 spectrophotometer.

Synthesis. 1,8-Bis(2,5-dihydroxybenzyl)-1,4,8,11-tetraazacyclotetradecane (H₄qp4). 1,4,8,11-Tetracyclotetradecane (cyclam; 1.00 g, 4.99 mmol) and 2,5-dihydroxybenzaldehyde (1.37 g, 9.91 mmol) were combined in 15 mL of dry MeOH. The mixture was heated at reflux for 4 h under N<sub>2</sub>. The reaction mixture was then cooled to 0 °C with an ice bath. Once the temperature reached 0 °C, 20 mL of additional dry MeOH and NaBH<sub>4</sub>/Al<sub>2</sub>O<sub>3</sub> (10 wt %, 0.83 g, ~0.02 mol) were gradually added to the solution. The resultant solution was heated at reflux for 6 h under N<sub>2</sub> and then cooled to 0 °C. The residual reductant was titrated with 1 M HCl until the solution reached pH 8, depositing the crude product as a solid, which was then collected via filtration. The solid was dissolved in acetone and filtered. The acetone was rotavaped to yield the product as a yellow powder (842 mg, 38% yield). Typical yields range from 38 to 42%. <sup>1</sup>H NMR (400 MHz, DMSO- $d_6$ , 297 K):  $\delta$  8.55 (s, 2H), 6.97 (s, 2H), 6.50– 6.56 (m, 4H), 6.45 (s, 2H), 3.16 (s, 4H), 2.45-2.59 (m, overlap with the solvent peak), 2.28 (s, 4H), 1.69 (s, 4H), 1.14 (s, 2H). <sup>13</sup>C NMR (100 MHz, DMSO- $d_6$ , 297 K):  $\delta$  149.98, 149.17, 124.98, 118.02, 117.10, 115.48, 53.80, 53.11, 50.50, 49.26, 46.38, 24.71. MS (ESI). Calcd for MH+: m/z 445.2815. Found: m/z 445.2821.

[1,8-Bis(2,5-dihydroxybenzyl)-1,4,8,11tetraazacyclotetradecane]manganese(II) triflate ([Mn(H<sub>3</sub>qp4)]-(OTf), 1). H<sub>4</sub>qp4 (500 mg, 1.12 mmol) and Mn(OTf)<sub>2</sub> (397 mg, 1.12 mmol) were dissolved in 5 mL of dried 1:1 MeCN/ tetrahydrofuran (THF) under N2. The mixture was stirred at 60 °C for 48 h; over this time, a green solid precipitated from the solution. The crude product was collected via filtration and washed with cold MeCN to yield the product as a green powder (577 mg, 76% yield). Typical yields range from 70 to 75%. MS (ESI). Calcd for  $[Mn(H_2qp4)]^+$ : m/z 497.1961. Found: m/z 497.1931. Calcd for  $[Mn(H_2qp4)(OTf)]^+$ : m/z 646.1481. Found: m/z 646.1470. Solidstate magnetic susceptibility (294 K):  $\mu_{\text{eff}} = 5.6 \, \mu_{\text{B}}$ . Optical spectroscopy (MeCN, 294 K): 300 nm (6800 M<sup>-1</sup> cm<sup>-1</sup>), 388 nm (3500 M<sup>-1</sup> cm<sup>-1</sup>). IR (cm<sup>-1</sup>): 3282 (m), 3069 (w), 2852 (w), 1611 (w), 1511 (m), 1483 (m), 1361 (m), 1279 (s), 1191 (s), 1238 (s), 1212 (s), 1180 (s), 1150 (s), 1090 (m), 1060 (m), 1026 (s), 992 (m), 916 (m), 868 (m), 815 (s), 751 (m), 631 (s), 572 (m), 510 (m).

Elem analy. Calcd for  $C_{25}H_{35}N_4O_7F_3S_1Mn\cdot 1.5H_2O$  (powder): C, 44.51; H, 5.67; N, 8.30. Found: C, 44.27; H, 5.14; N, 8.09.

### RESULTS

Synthesis and Nonaqueous Characterization. The  $H_4qp4$  ligand is synthesized in one step from cyclam, 2 equiv of 2,5-dihydroxybenzaldehyde, and excess  $NaBH_4/Al_2O_3$  (Scheme 2). The synthesis was inspired by that used to

## Scheme 2. Synthesis of H<sub>4</sub>qp4

prepare 1,8-bis(2-hydroxybenzyl)-1,4,8,11-tetraazacyclotetradecane ( $H_2$ bcyclamb), which features phenols in place of the quinol groups. The preparation of  $H_4$ qp4 is complicated by the sensitivity of the bisaminal intermediate to air, necessitating that the addition of the quinols be done in a one-pot reaction rather than over two discrete steps. The one-pot reaction has the unexpected benefit of modestly improving the yield of  $H_4$ qp4 (38%); the overall yield of  $H_2$ bcyclamb was 28%. The purity and identity of  $H_4$ qp4 were confirmed by NMR and HR-MS. We also crystallized the triflic acid salt of the ligand,  $[H_6$ qp4](OTf)<sub>2</sub>, from MeOH (Figure 1).

A Mn(II) complex with  $H_4$ qp4, [Mn( $H_3$ qp4)](OTf) (1), can be prepared by refluxing the ligand and Mn(OTf)<sub>2</sub> in 1:1 MeCN/THF for 2 days. The complexation reaction requires a much higher temperature and a much longer reaction time than the syntheses of [Mn( $H_2$ qp1)(MeCN)](OTf)<sub>2</sub> (2) and 3.<sup>7,8</sup> The incorporation of metal ions into macrocycles often requires such measures. Complex 1 differs from previously isolated Mn(II) complexes with polydentate quinol-containing ligands in that it features a deprotonated quinol. Elemental analysis of powdered samples of 1 indicates that there is a single triflate per manganese. Both the EPR and magnetic susceptibility measurements indicate that the metal ion is high-

spin Mn(II). Because there is only one counteranion, this thereby necessitates a 1- charge on the polydentate ligand ( $H_3qp4^-$ ). The presence of a quinolate is further supported by the presence of two bands in the UV/vis spectrum of the isolated product in MeCN (Figure S6). The feature at 304 nm is consistent with a neutral quinol; bands at similar energies are the sole UV/vis features observed above 250 nm for both 2 and 3 in MeCN. The additional band at 388 nm has an energy that is more consistent with a quinolate group; these have been observed for the  $H_2qp1$  and  $H_4qp2$  complexes in water.

Complex 1 is stable to air in the solid and solution states for prolonged periods of times. Samples of 1 in MeCN display negligible changes to their UV/vis features over a 12 h exposure to air (Figure S6). If solutions of 1 in either aqueous or organic solvents are kept under air for 1-2 weeks, the compound does eventually oxidize to  $[Mn^{III}(H_2qp4)](OTf)$  (4), where  $H_2qp4^{2-}$  is the doubly deprotonated form of the ligand.

Structures of  $[H_6qp4](OTf)_2$  and 4. The crystal structure of the doubly protonated  $H_4qp4$  ligand is shown in Figure 1A. The protonation state of the ligand was deduced from the 1:2 ligand/triflate ratio of the solid. Each additional proton bridges the two nitrogen atoms from a 1,2-ethanediamine portion of the macrocycle. One of the oxygen atoms from the nearest quinol is centered over each 1,2-ethanediamine moiety, with nearly equal distances between the oxygen atom and each nitrogen atom (2.94 and 2.95 Å).

Attempts to crystallize 1 have thus far been unsuccessful, but we crystallized 4 by slowly diffusing CH<sub>2</sub>Cl<sub>2</sub> into a saturated solution of 1 in MeCN under air over 2 weeks (Figure 1). The reddish color of the crystals suggests that the manganese has been oxidized to either the 3+ or 4+ oxidation state. Single-crystal X-ray diffraction data unambiguously assign the metal center as Mn(III). The Mn–N and Mn–O bonds for 4 average 2.16 and 1.89 Å, respectively. Typical bonds between Mn(II) and neutral nitrogen donors are longer, ranging from 2.2 to 2.3 Å, and bonds between Mn(II) and even anionic oxygen donors usually exceed 2.0 Å. 6-8,20,26-28 The Mn–N and Mn–O bond distances observed for 4 are instead more consistent with a Mn(III) ion bound to neutral nitrogen donors and anionic oxygen donors. Additionally, the coordination complex displays a rhombic [2+2+2] Jahn–Teller distortion, with pairs of short [Mn–O(1) and Mn–

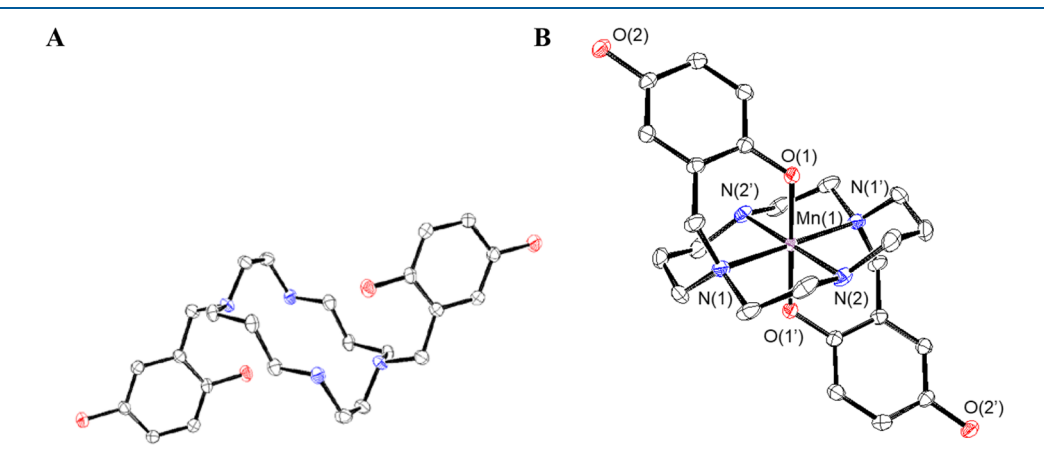


Figure 1. ORTEP representations of (A)  $[H_6qp4]^{2+}$  and (B)  $[Mn(H_2qp4)]^+$  (4). All hydrogen atoms, solvent molecules, and counteranions have been removed for clarity. All ellipsoids depict 50% probability.

Table 2. pMn, log K<sub>MI</sub>, and pK<sub>a</sub> Values Determined by Potentiometric Titration at 25 °C

$pK_{L1}^{a}$	3.50 (±0.05)	$\log K_{\rm ML}[{\rm Mn}({\rm H_2qp4})]^c$	20.85
$pK_{L2}^{a}$	$7.70 (\pm 0.05)$	$\log K_{\rm ML}[Mn(H_3qp4)^+]^c$	18.22
$pK_{L3}^{a}$	8.80 (±0.05)	$\log K_{\rm ML}[\rm Mn(H_4qp4)^{2+}]^c$	14.52
$pK_{L4}^{a}$	10.02 (±0.05)	pMn (pH 7.4) <sup>d</sup>	9.81
$pK_a[Mn(H_4qp4)^{2+}]^b$	5.09 (±0.05)		
$pK_1[Mn(H_2qp4)^+]^b$	7.39 (+0.05)		

"Ligand pK<sub>a</sub> values:  $K_{L1} = [H_3qp4^+][H^+]/[H_6qp4^{2^+}]; K_{L2} = [H_4qp4][H^+]/[H_3qp4^+]; K_{L3} = [H_3qp4^-][H^+]/[H_4qp4]; K_{L4} = [H_2qp4^{2^-}][H^+]/[H_3qp4^-].$  "Metal complex pK<sub>a</sub> values:  $K_a[Mn(H_4qp4)^{2^+}] = [Mn(H_3qp4)^+][H^+]/[Mn(H_4qp4)^{2^+}]; K_a[Mn(H_3qp4)^+] = [Mn(H_2qp4)][H^+]/[Mn(H_3qp4)^+].$  "Metal complex  $K_{ML}$  values:  $K_{ML}[Mn(H_2qp4)] = [Mn(H_2qp4)]/([Mn(II)][H_2qp4^{2^-}]); K_{ML}[Mn(H_3qp4)^+] = [Mn(H_3qp4)^+]/([Mn(II)][H_3qp4^-]); K_{ML}[Mn(H_4qp4)^{2^+}] = [Mn(H_4qp4)^{2^+}]/([Mn(II)][H_4qp4]).$  "pMn =  $-\log [Mn(II)]_{free}$  calculated for [Mn(II)] = 1.0 mM, [H\_4qp4] = 1.0 mM, 298 K, pH 7.4.

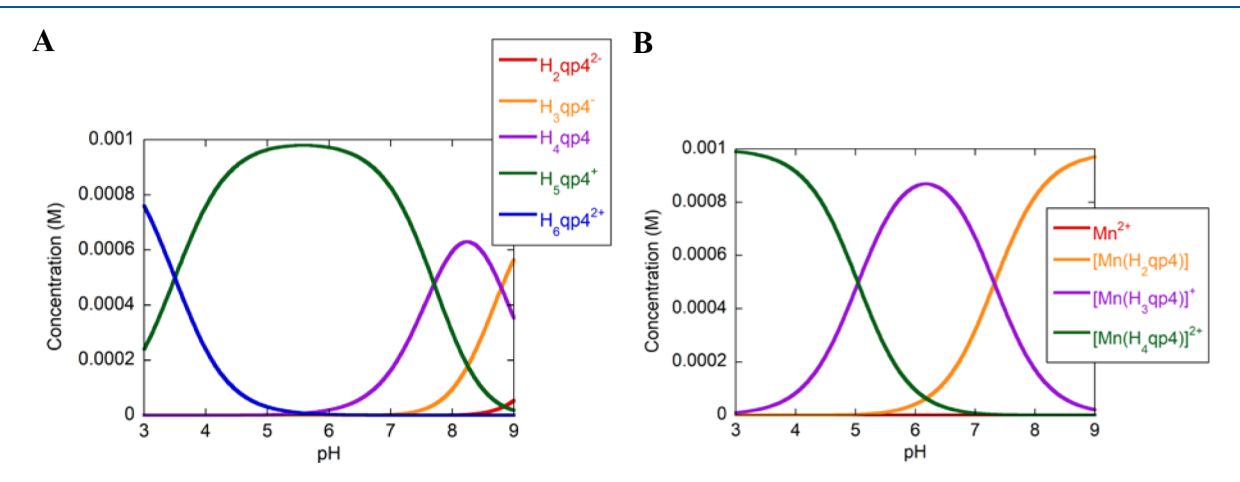


Figure 2. Predicted speciation as a function of the pH for (A) 1.0 mM  $H_4$ qp4 and (B) a 1:1 mixture of  $H_4$ qp4 and MnCl<sub>2</sub> in a 100 mM KCl solution.

O(1')], intermediate [Mn-N(2) and Mn-N(2')], and long [Mn-N(1) and Mn-N(1')] metal-ligand bonds. Such distortions would be anticipated for a high-spin  $d^4$  electronic configuration but not for a  $d^3$  metal ion. The metal center is therefore more likely to be Mn(III) than Mn(IV).

**Stability and Speciation of 1 in Water.** The speciation of the free  $H_4$ qp4 ligand was investigated from pH 3 to 9 (Figure S7). The best-fitting model to the potentiometric pH titration data is comprised of four ionization events corresponding to  $pK_a$  values of 3.5, 7.7, 8.8, and 10.0 (Figure S8 and Tables S1 and 2). Cyclam by itself is quadruply protonated under extremely acidic conditions, with two of the protons being retained from pH 2 to  $10.^{30}$  The  $H_4$ qp4 ligand appears to behave similarly, and the species at pH 3 is assigned as  $H_6$ qp4<sup>2+</sup>. The ligand exists primarily as  $H_5$ qp4<sup>+</sup> at pH 7.0, with a considerable amount of  $H_4$ qp4 (Figure 2A). Traces of doubly deprotonated  $H_2$ qp4<sup>2-</sup>, which would feature two quinolates, are seen at the basic end point of the titration.

The inclusion of a macrocycle into the ligand framework greatly stabilizes 1 in water relative to previously prepared contrast agents from our laboratory. The stability and speciation of 1 were assessed using potentiometric pH titration data acquired from pH 3 to 9. Our best-fitting model for the data suggests that there is negligible Mn(II) release from the ligand even at pH 3 (Figure S9, Figure 2B). The pMn at pH 7.4 with 1.0 mM of Mn(II) and ligand is calculated to be 9.81. Two ionization events are observed between pH 3.0 and 9.0. The associated p $K_a$  values of 5.09 and 7.39 are consistent with the sequential deprotonation of two Mn(II)-bound quinols as the solution is made more basic. 8,12,31 The calculated log  $K_{\rm ML}$  values for Mn(II) bound to  $H_4$ qp4,  $H_3$ qp4<sup>-</sup>, and  $H_2$ qp4<sup>2-</sup> all

exceed 14, with the binding affinity becoming stronger as the ligand deprotonates to more anionic forms.

The stability of the Mn(II)-H<sub>4</sub>qp4 complex in water is confirmed by HPLC (Figures S10 and S11). The H<sub>4</sub>qp4 ligand and 1 each give rise to single LC peaks with distinct retention times. Partial deprotonation of the metal-bound quinols in 1 at pH 7.00 is supported by UV/vis measurements. The spectrum of 1 in a 50 mM HEPES solution buffered to pH 7.00 displays an intense band at 388 nm that is absent in the spectrum for metal-free  $H_4$ qp4 under the same conditions (Figure S12). The energy of this new band is consistent with a phenolate or quinolate group. The assignment of the 5.09 and 7.39 p $K_a$ values to deprotonation of the metal-bound quinols is also supported by a parallel spectrophotometric pH titration (Figure S13). The UV/vis spectrum of 1 changes markedly and continually as the pH rises from 4 to 9. Because Mn(II) does not generally support charge-transfer or d-d bands, these changes can be assigned to sequential deprotonation of the ligand's two quinols.

Complex 1 was electrochemically characterized by CV in an aqueous 50 mM phosphate solution buffered to pH 7.2. An irreversible feature with  $E_{\rm pa}=1.25$  V versus Ag/AgCl was observed and assigned to the oxidation of the metal to Mn(III). In addition, we also detect a redox feature with  $E_{1/2}=100$  mV versus Ag/AgCl (295 mV vs NHE; Figure S14). The separation between the anodic and cathodic peaks ( $\Delta E$ ) is approximately 260 mV. Because redox processes with similar  $E_{1/2}$  values were found for manganese and zinc complexes with polydentate quinol-containing ligands, we tentatively assign the 100 mV versus Ag/AgCl feature to the oxidation and reduction of the ligand rather than the manganese. <sup>7,8,32</sup> The  $\Delta E$  value for

the 100 mV redox event is larger than the 230 mV value measured for 3; we attribute the poor reversibility of both features to the more extensive acid/base chemistry associated with having two, rather than one, quinol/quinolate groups in these coordination complexes.

The ability of 1 to interact with water was studied using variable-temperature <sup>17</sup>O NMR using the methodology pioneered by Gale et al. (Figure 3). <sup>19</sup> The results at pH 7.4

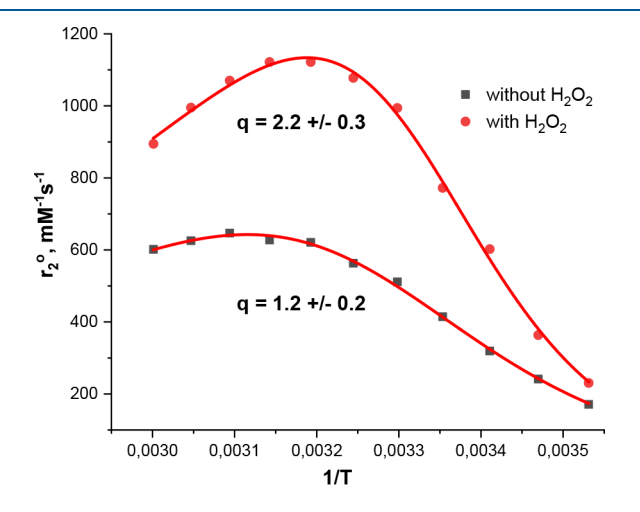


**Figure 3.** Plots of  $r_2^{\circ}$  as a function of the temperature for 1 before and after oxidation by  $H_2O_2$ . Experimental conditions for the preactivated sensor (black squares): [1] = 6.0 mM in 60 mM HEPES buffered to pH 7.4 and 10% (v/v) of 10%  $^{17}OH_2$ , and B=9.4 T. Experimental conditions for the activated sensor (red circles): [1] = 2.5 mM in 60 mM MOPS buffered to pH 7.4 with 15 equiv of  $H_2O_2$  and 10% (v/v) of 10%  $^{17}OH_2$ , and B=9.4 T. We began to acquire NMR data 15 min after the start of the oxidation reaction.

are consistent with q=1.2 (Table 3). When 1 is dissolved in pH 7.4 water, the predominant species is therefore [Mn- $(H_3qp4)(H_2O)$ ]<sup>+</sup>, with the next most prevalent species being [Mn( $H_2qp4$ )( $H_2O$ )]. The calculated rate constant for water exchange at 298 K is  $1.7 \times 10^7$  s<sup>-1</sup>, which is at the slower end of the range typically seen for Mn(II) complexes. 8,19,34–40  $\Delta S^{\ddagger}$  is highly positive, consistent with a dissociate mechanism for water exchange at the metal center.

Stability of 1 to Air and Adventitious Metal lons. Complex 1 does not display any noticeable short-term reactivity to air. The UV/vis spectrum of 1 in MeCN does not appreciably change over the course of a 12 h exposure to air (Figure S6). Both 2 and 3, conversely, appear to oxidize slightly (5–10%) to manganese(II) p-quinone complexes under the same conditions.  $O_2$  does eventually oxidize 1, with the Mn(III)-containing 4 depositing over 1–2 weeks (Figure 1B).

Complex 1 differs from 2 and 3 in that it strongly resists metal-ion exchange. The reaction between 0.1 mM  $\rm Fe(ClO_4)_2$ 

and 0.1 mM 1 in either MeCN or buffered water does not yield UV/vis-detectable quantities of [Fe(H<sub>3</sub>qp4)]<sup>+</sup>, even at 18 h (Figure S15). The changes to the UV/vis spectrum of 1 over this time are negligible. Complex 2, conversely, slowly exchanges Fe(II) for Mn(II) in MeCN, with approximately 10% of the Mn(II) being displaced by an equimolar amount of Fe(II) by 15 h. Complex 3 is the most susceptible of the three manganese(II) quinol complexes to metal-ion displacement, and 80% of its Mn(II) is displaced by an equimolar amount of Fe(II) by 3 h.8 Both the H<sub>2</sub>qp1 and H<sub>4</sub>qp2 complexes with Mn(II) react readily with Zn(II), with the strong diamagnetic <sup>1</sup>H NMR features of the Zn(II)-H<sub>2</sub>qp1 and Zn(II)-H<sub>4</sub>qp2 complexes appearing within 2 h.  $^{7/8}$  The reactions between 20 mM  $Zn(ClO_4)_2$  and 10 mM 1 in  $CD_3CN$  or  $D_2O$ , however, fail to dislodge Mn(II) from the ligand, as assessed by <sup>1</sup>H NMR (Figure S16). The <sup>1</sup>H NMR spectra of the reactions are featureless aside from solvent peaks even 24 h after the introduction of the Zn(II). When 20 mM H<sub>2</sub>O<sub>2</sub> is added to a mixture of 20 mM Zn(ClO<sub>4</sub>)<sub>2</sub> and 10 mM 1, Mn(II) likewise remains in the oxidized forms of the ligand (H<sub>2</sub>qp4 and qp4, Scheme 3), as assessed by <sup>1</sup>H NMR.

Scheme 3. Oxidized Forms of the H<sub>4</sub>qp4 Ligand

**Reactivity between 1 and H\_2O\_2.** Upon reaction with 2,3-dichloro-5,6-dicyano-1,4-benzoquinone (DDQ), the quinols in 1 appear to be partially oxidized to *p*-quinones, as assessed by MS, UV/vis, and IR (Scheme 3 and Figures S17–S19). A new IR feature at 1656 cm<sup>-1</sup> provides strong evidence for formation of the C=O bonds associated with *p*-quinone.

When 1 reacts with a large 10 mM excess of  $H_2O_2$ , MS reveals m/z features similar to those seen for oxidation of the Mn(II) complex by DDQ, suggesting that the quinols are likewise converted to p-quinones by this oxidant (Figure S20). Further investigation reveals that the speed of the reaction between 1 and excess  $H_2O_2$  is significantly slower than analogous reactions with 2 and 3.<sup>7,8</sup> Curiously, the changes to the optical spectra during the first 30 min are slight, consistent with an induction period (Figure 4A). The reaction then

Table 3. Water-Exchange Activation Parameters Obtained for Quinol-Containing Mn(II) Complexes 1-3

parameter	1 (pH 7.4)	1 (pH 7.4) after oxidation	2 (pH 7.4) <sup>a</sup>	3 (pH 7.0) <sup>b</sup>
q	1.2 (±0.2)	2.2 (±0.3)	0.7 (±0.2)	0.9 (±0.2)
$k_{\rm ex}^{298}  ({\rm s}^{-1})$	$1.7 \ (\pm 0.1) \times 10^7$	$1.6 \ (\pm 0.4) \times 10^7$	$6.9 \ (\pm 0.6) \times 10^7$	$4.9 \ (\pm 1.4) \times 10^6$
$\Delta H^{\ddagger}$ (kJ mol <sup>-1</sup> )	45 (±2)	50 (±9)	24.2 (±1.0)	22.0 (±1.7)
$\Delta S^{\ddagger}$ (J K $^{-1}$ mol $^{-1}$ )	43 (±6)	62 (±11)	$-13.1 \ (\pm 3.4)$	$-41 \ (\pm 2)$

<sup>&</sup>lt;sup>a</sup>From ref 33. <sup>b</sup>From ref 8.

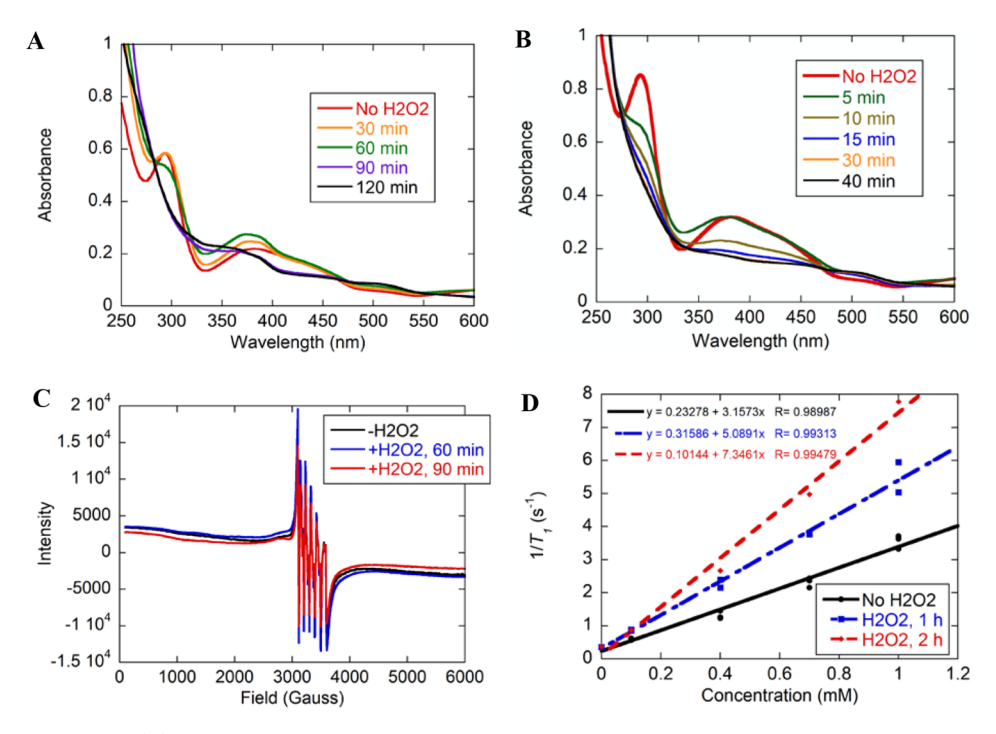


Figure 4. Response of 1 to  $H_2O_2$ . (A) UV/vis spectra acquired during a reaction between 0.07 mM 1 and 10 mM  $H_2O_2$  in 50 mM HEPES buffered to pH 7.00 at 298 K. (B) UV/vis spectra acquired during a reaction between 0.10 mM 1 and 0.60 mM  $H_2O_2$  in 50 mM HEPES buffered to pH 7.00 at 298 K. (C) X-band EPR spectra of 1.0 mM solutions of 1 in 50 mM HEPES buffered to pH 7.00 in the absence and presence of 10 mM  $H_2O_2$ . The reactions between 1 and  $H_2O_2$  proceeded for 60 min (blue) and 90 min (red) before the samples were frozen and analyzed at 77 K. (D) Plots of  $1/T_1$  versus Mn(II) concentration for 1 in the presence (blue, red) and absence (black) of 10 mM  $H_2O_2$ . All samples were run in 298 K aqueous solutions containing 50 mM HEPES buffered to pH 7.00, using a 3 T field provided by a clinical MRI scanner. All samples were prepared under air. The oxidized samples were prepared by directly adding  $H_2O_2$  to solutions of 1 in aqueous solutions buffered to pH 7.0. Two sets of oxidation reactions were allowed to proceed for 60 min at 298 K before  $T_1$  was measured (blue). A third set of oxidation reactions was allowed to proceed for 120 min before data acquisition. The data were fit to the indicated linear equations. The y intercepts were within error of  $1/T_1$  measurements associated with two control samples that contained no Mn(II): pure water (0.35 s<sup>-1</sup>) and 50 mM HEPES buffer (0.34 s<sup>-1</sup>).

accelerates and finishes by 90 min. The most noticeable optical changes are the disappearance of the peaks at 293 and 388 nm; features with similar energies have been observed for 2 and 3 and assigned to intraligand transitions for the quinol and quinolate moieties. When a smaller amount of  $\rm H_2O_2$  (0.6 mM) is added to 1, the quinol peak decreases immediately, with the reaction completing in 20 min (Figure 4B), indicating that the induction period only occurs when  $\rm H_2O_2$  is present in a large excess.

When the reaction between 1.0 mM 1 and 10 mM  $H_2O_2$  in a pH 7.0 HEPES buffer is monitored by EPR, the spectrum taken before the oxidant was added looks nearly identical with those taken at 60 and 90 min, suggesting that the manganese largely remains in the 2+ oxidation state throughout the reaction (Figure 4C). As with prior quinol-containing  $H_2O_2$  sensors from our laboratory, not all of the quinols are oxidized to p-quinones by excess  $H_2O_2$ .<sup>7,8</sup> The Mn(II) exists as a mixture of unreacted 1,  $[Mn(Hqp4)]^+$ , and  $[Mn(qp4)]^{2+}$ , where  $Hqp4^-$  and qp4 correspond to the mono-p-quinone/quinolate and di-p-quinone oxidized forms of the ligand. Oxidation of the quinols is potentially reversible. When 1 is oxidized by  $H_2O_2$  in MeOH, we can regenerate the  $H_3qp4^-$  complex by subsequently adding sodium dithionite (Figure S21).

Upon oxidation by  $H_2O_2$ , the aquation number of the Mn(II) center in 1 increases by approximately one water molecule, resulting in an average of 2.2 water molecules binding to each metal center (Figure 3 and Table 3). The rate

of water exchange does not significantly change, with the rate constant being identical within error with that measured before oxidation.  $\Delta S^{\ddagger}$  for water exchange remains highly positive after the reaction with  $H_2O_2$ , suggesting that this process still occurs through a dissociative pathway.

MRI Properties. The relaxivities of complex 1 before and during its reaction with  $H_2O_2$  were assessed using a 3 T MRI scanner (Figure 4D).  $T_1$  values were measured for aqueous solutions containing 0–1.0 mM 1 and 50 mM HEPES buffered to pH 7.00. For each concentration of 1, an oxidized sample was also prepared by adding 10 mM  $H_2O_2$ ; the large excess of oxidant was used to ensure as full a turn-on as possible at the time points and to facilitate comparisons to manganese-containing MRI contrast agents that were previously prepared and characterized by our laboratory. The  $T_1$  values for the  $H_2O_2$ -containing solutions were measured 1 and 2 h after the reagents were initially mixed. Full series of data were collected for two independently prepared batches of 1 in order to confirm that the results were replicable.

Relaxivities  $(r_1)$  were obtained from the slopes of plots of  $1/T_1$  versus manganese concentration. Prior to oxidation by excess  $H_2O_2$ ,  $r_1$  was 3.16 mM<sup>-1</sup> s<sup>-1</sup>. The data taken for samples kept under air for 1 and 2 h overlay well, suggesting that the short-term reactivity with air is slight. After oxidation by  $H_2O_2$ , the relaxivity rises, reaching 5.09 mM<sup>-1</sup> s<sup>-1</sup> by 1 h and peaking at 7.35 mM<sup>-1</sup> s<sup>-1</sup>, as assessed by measurements taken at 2 h (Figure 4D). The pH dependence of the relaxivity was investigated from pH 3 to 9 (Figure S22). The  $r_1$  values were

Scheme 4. Other Mn(II)-Binding Ligands Used in MRI Contrast Agents

measured for a 0.50 mM sample of 1.  $r_1$  is highest at pH 3 and lowest at pH 7. As the pH increases,  $r_1$  drops from pH 3 to 4, remains approximately constant from pH 4 to 6.5, decreases from pH 6.5 to 7, and then rises slightly from pH 7 to 9.

#### DISCUSSION

Both H<sub>4</sub>qp4 and 1 were prepared in straightforward manners using techniques slightly modified from previously successful procedures. The synthesis for a closely related cyclam derivative with two phenols appended to two of the amines was done in two distinct steps, 25 but the heightened air sensitivity of the quinols under basic conditions led us to explore and eventually adopt a one-pot reaction. Once the ligand was prepared, the installation of Mn(II) into the macrocycle proceeded cleanly using protocols commonly used for other macrocycle complexation reactions. 41-44 Unexpectedly, Mn(II) is bound to the singly deprotonated ligand H<sub>3</sub>qp4<sup>-</sup>, rather than neutral H<sub>4</sub>qp4, in the solid isolated from precipitation of the Mn(II) complex from organic solvents. Analogous complexes with  $H_2qp1$  and  $H_4qp2$  (Scheme 1), 2 and 3, contain exclusively quinols rather than quinolates.<sup>7,8</sup> We speculate that residual metal-free H<sub>4</sub>qp4 may serve as the base that deprotonates the metal-bound ligand. Although we have not isolated the protonated ligand byproduct(s), we feel that this is a likely explanation for deprotonation of the Mn(II) complex because of the ligand's high affinity for protons and the ~75% yield of 1, which would provide enough residual ligand to serve as a base.

As anticipated, 1 contains a high-spin Mn(II) metal center, as evidenced by EPR, UV/vis, and solid-state magnetic susceptibility data. The UV/vis features correspond to intraligand transitions for the quinol and quinolate groups; these provide convenient spectroscopic signatures to follow the oxidation state of the ligand.<sup>7–9</sup>

Complex 1 is much more thermodynamically stable in water than the previously characterized 3, which has a similar coordination sphere around the metal center in aqueous solution. The pMn value measured at pH 7.4 with 1.0 mM concentrations of the ligand and Mn(II) is 9.81, which represents over 4 orders of magnitude of improvement over the 5.36 value measured for 3. The gains in stability can be attributed largely to macrocyclic effects because  $H_4$ qp2 and  $H_4$ qp4 provide similar coordination spheres: four neutral nitrogen donors in addition to the two quinols/quinolates. Complex 1 is also more stable than 2, which has a pMn of 7.25 under our standard conditions.

The stability of 1 also exceeds those of most other reported mononuclear Mn(II)-containing MRI contrast agents.  $^{9,14,37,39,40,45-48}$  The Gale and Caravan groups have recently reported a series of linear ligands with multiple carboxylate donors that coordinate tightly to Mn(II).  $^{37,46}$  One

representative example, PyC3A³-, forms a Mn(II) complex with a log  $K_{\rm ML}$  of 14.14 (Scheme 4).³7 The H<sub>6</sub>qc1 ligand (Scheme 1) was inspired by this work, and the triply deprotonated H<sub>3</sub>qc1³- forms a Mn(II) complex with a log  $K_{\rm ML}$  of 15.59.9 The log  $K_{\rm ML}$  values for the Mn(II) complexes with H<sub>2</sub>qp4²- and H<sub>3</sub>qp4<sup>-</sup> both exceed 18, demonstrating that the macrocycle can stabilize Mn(II) complexes more efficiently than more highly anionic linear ligands. The DOTA⁴- ligand represents a combination of these strategies in that it is comprised of four carboxylates tethered to a cyclen framework (Scheme 4). The log  $K_{\rm ML}$  value for its Mn(II) complex (19.89) is higher than the 18.22 value for H<sub>3</sub>qp4<sup>-</sup> but less than the 20.85 value measured for H<sub>2</sub>qp4²-.⁴³,⁴³ The 19.01 log  $K_{\rm ML}$  value for the Mn(II) complex with the macrocyclic PC2A-EA²- (Scheme 4) is also similar to that of 1.⁴0

Inclusion of the cyclam into the ligand also endows 1 with a high level of kinetic stability as assessed by metal competition experiments. Once in the macrocycle, Mn(II) cannot be facilely displaced by either Fe(II) or Zn(II), two of the most common transition-metal ions in biology. Complexes 2 and 3, conversely, gradually react with equimolar amounts of free Fe(II) and quickly react with Zn(II). The inertness of 1 toward metal-ion exchange compares well to those of other Mn(II)containing MRI contrast agents with macrocyclic organic components. 14,40,44 The kinetic stability extends to Mn(II) complexes with oxidized forms of the H<sub>4</sub>qp4 ligand. Oxidation by H<sub>2</sub>O<sub>2</sub> yields a mixture of Mn(II) complexes with the monoquinol/monoquinone and diquinone ligands H<sub>2</sub>qp4 and qp4 (Scheme 3). <sup>1</sup>H NMR analysis of the reaction between these oxidized complexes and Zn(II) reveals that Zn(II) does not noticeably displace Mn(II). The oxidized forms of complex 3, conversely, exchange Zn(II) for Mn(II) under these conditions, leading to intense diamagnetic peaks when visualized by NMR.

Like 2 and 3, 1 is a redox-active  $T_1$ -weighted MRI contrast agent. Curiously, the preoxidation relaxivity of 1 (3.15 mM<sup>-1</sup>  $s^{-1}$ ) is much lower than that of 3 (5.46 mM<sup>-1</sup> s<sup>-1</sup>), despite the two compounds having similar coordination spheres and acid/ base behavior. Both  $r_1$  values are the weighted averages of the relaxivities of the individual Mn(II) species present at pH 7.00:  $[Mn(H_3qp4)(H_2O)]^+$  and  $[Mn(H_2qp4)(H_2O)]$  in the case of 1. The average aquation number measured for 1 is slightly higher than that of 3, but this would be anticipated to raise rather than lower the  $r_1$ . The p $K_a$  values for the two Mn(II)bound quinols in 1 and 3 are also similar: 5.82 and 7.14 for 3 versus 5.09 and 7.39 for 1. The higher p $K_a$  value in each pair would be anticipated to modulate the rate of proton transfer.<sup>49</sup> The slightly more basic quinolate in 1 could slow the rate of proton transfer between the manganese(II) quinols and the bulk water enough to substantially reduce its contribution to the measured  $r_1$ , but further studies are needed to fully

elucidate that possible relationship. The rate constants for water exchange at 298 K differ the most, with the  $k_{\rm ex}$  value measured for 3 (4.9 × 10<sup>6</sup> s<sup>-1</sup>) being approximately a third of that of 1 (1.7 × 10<sup>7</sup> s<sup>-1</sup>). Complex 1, unlike 3, appears to exchange water molecules through a dissociative mechanism, as evidenced by the highly positive entropy of activation (Table 3).

The relaxivity measured for nonoxidized 1, like that of 3, is higher under acidic conditions (Figure S22). This may be consistent with water molecules displacing the quinol portions of the ligand from the metal. Alternatively, protonation of the quinolate groups under more acidic conditions may increase the relaxivity by enabling more extensive exchange with the protons from the bulk water. As the pH becomes more basic, the metal-bound quinols deprotonate to anionic quinolates that can outcompete water for coordination sites on the metal center.

In addition to the higher stability, the inclusion of cyclam in the ligand framework has the nonintuitive benefit of improving the relaxivity response to  $H_2O_2$ . The 130% increase in  $r_1$  is approximately quadruple the percentile increase observed for 3.8 Complex 3 rapidly destabilizes as the pH drops below 7.0 because of the protonation of manganese(II) quinolates, and it is reasonable to assume that oxidation of the quinols to pquinones likewise weakens the binding affinity of the ligand enough to trigger release of the Mn(II). The H<sub>2</sub>O<sub>2</sub>-enhanced  $r_1$  for 3, however, cannot be attributed to release of the metal. The  $r_1$  of  $[Mn(H_2O)_6]^{2+}$  was measured independently (5.26 mM<sup>-1</sup> s<sup>-1</sup>) and found to be approximately equal to that of the preactivated form of 3 (5.46 mM<sup>-1</sup> s<sup>-1</sup>). 8,20 Although one may expect  $[Mn(H_2O)_6]^{2+}$  to have a higher  $r_1$  because of its higher aquation number, this is not observed. Proton exchange between water molecules and the Mn(II)-bound quinols/ quinolates would be anticipated to markedly increase the  $r_1$ values of 1-3 relative to q = 1 systems that lack metal-bound hydroxyl groups from their organic ligands. 49 Counterintuitively, Mn(II)-ion release from the oxidized forms of  $H_4$ qp2 may actually curtail the response of 3 to  $H_2O_2$ .

If 1 were to release free Mn(II) upon oxidation, we would anticipate an increase in  $r_1$  due to the lower starting value, but this mechanism is not consistent with our data. Our NMR measurements indicate that the oxidation of 1 by  $H_2O_2$  does not release significant amounts of Mn(II). Further, the maximum  $r_1$  exceeds that of  $[Mn(H_2O)_6]^{2+}$ . We instead believe that the increase in relaxivity results from the formation of more highly aquated Mn(II) species with the oxidized forms of the ligand. Because the H2O2 reaction does not make either  $[Mn(Hqp4)(H_2O)_x]^+$  or  $[Mn(qp4)(H_2O)_x]^{2+}$  cleanly, we unfortunately cannot measure the individual  $r_1$  values of these two species and ascertain their contributions to the overall relaxivity. Oxidation by H2O2 does improve the aquation of the metal center, as evidenced by variabletemperature <sup>17</sup>O NMR measurements (Table 3 and Figure 3). On average, the metal centers coordinate one additional water molecule after oxidation.

Complex 1 differs substantially from 2 and 3 in that its response to  $\rm H_2O_2$  depends on the manner in which the oxidant is administered. When a large excess of  $\rm H_2O_2$  is added to 1 in a single portion, oxidation of the quinols occurs after an induction period. The oxidation by 10 mM  $\rm H_2O_2$  takes approximately 90 min to complete, as assessed by changes to both the relaxivity and UV/vis spectrum. When a smaller portion of  $\rm H_2O_2$  is added, the quinols are oxidized more

quickly and without a noticeable induction period. On the basis of these observations, we propose that the initial reaction between  $H_2O_2$  and 1 generates an oxidant that can react either unimolecularly to oxidize one of the quinols to p-quinone or bimolecularly with another equiv of  $H_2O_2$  to yield  $O_2$  and regenerate 1 (Scheme 5). In high concentrations of  $H_2O_2$ , the

Scheme 5. Proposed Competing Catalase and Quinol Oxidation Pathways

LMn<sup>II</sup> OH

H<sub>2</sub>O<sub>2</sub>

H<sub>2</sub>O<sub>2</sub>

H+ {O-O heterolysis}}

H<sub>2</sub>O<sub>2</sub>

$$H_{2}$$
OH

 $H_{2}$ OH

second pathway dominates, and the manganese complex primarily acts as a catalase mimic. Complexes 2 and 3, conversely, quickly react with excess H<sub>2</sub>O<sub>2</sub> to yield manganese-(II) p-quinone complexes, and these reactions do not feature induction periods. We speculate that efficient oxidation of quinols to para-quinones may require that the quinols be cis to the H<sub>2</sub>O<sub>2</sub>-derived ligand in a transient higher-valent intermediate, which we depict as a manganese(IV) oxo complex in Scheme 5. If the macrocycle coordinates the manganese in a square-planar fashion as it does to the Mn(III) in 4 (Figure 1B), an incoming H<sub>2</sub>O<sub>2</sub> will likely displace a quinol/quinolate, forcing the H<sub>2</sub>O<sub>2</sub>-derived ligand to be trans to the remaining metal-bound quinol/quinolate. This would hinder intramolecular oxidation and enable bimolecular reactions with additional equivalents of H<sub>2</sub>O<sub>2</sub> to proceed. A similar hindrance of intramolecular quinol oxidation may also explain the reaction between 1 and O2. The product of this reaction is 4 (Figure 1B) rather than a Mn(II) complex with a p-quinone-containing ligand, the latter of which might be anticipated to be more thermodynamically stable based on the electrochemistry (Figure S14).

Preliminary data suggest that 1 can indeed catalyze the degradation of  $H_2O_2$ . When reactions between 100 nM 1 and 10 mM  $H_2O_2$  are followed spectrophotometrically, the absorbance of the  $H_2O_2$  peak at 240 nm decreases quickly (Figure S23). From these data, the initial rate,  $\nu_0/[1]_T$ , was estimated to be 6.6 ( $\pm 2.3$ )  $\times$  10<sup>3</sup> s<sup>-1</sup>.

Biological environments generally provide low but rapidly replenishing concentrations of  $\rm H_2O_2$  that are closer to 0.6 mM than 10 mM.  $^{50-52}$  We therefore anticipate that 1 would provide a fast  $r_1$  response to physiologically generated  $\rm H_2O_2$  that is more similar to that displayed in Figure 4B than in Figure 4A. Even with this in mind, it is uncertain whether the sensor will respond quickly enough to an oxidant to activate before circulating out of an area with elevated levels of  $\rm H_2O_2$ . Other challenges exist in translating probes such as 1 to the

clinic. The nonratiometric response of 1, for instance, makes it difficult to distinguish regions under oxidative stress from sites that merely accumulate more of the preactivated sensor. Although 2 and 3 seem to be reasonably tolerated by cells, <sup>7,8</sup> the potential toxicity of 1 also needs to be considered and assessed.

#### CONCLUSIONS

A Mn(II) complex with a cyclam macrocycle derivatized with two quinols is a highly water-stable MRI contrast agent that displays a positive  $r_1$  response to  $H_2O_2$ , one of the most prevalent ROS in biology. The percentile relaxivity response is approximately four times that of a Mn(II) complex with a linear ligand that provides a similar set of donor atoms: two quinols/quinolates and four neutral nitrogen donors. In addition to boosting the thermodynamic stability, the macrocycle also provides a kinetic barrier for metal-ion dissociation, and the Mn(II) complex appears to retain the metal after oxidation of the quinols to more poorly metal-binding pquinones. The greater stability of the current complex addresses a key concern about other quinol-containing MRI contrast agent sensors that were previously prepared by our laboratory and should smooth the pathway toward using such complexes to monitor biologically relevant oxidative stress.

The reactivity with  $H_2O_2$  appears to proceed through two competing pathways. With low  $H_2O_2$  levels, intramolecular oxidation of the quinols to p-quinones occurs. This process appears to be slow relative to analogous reactions seen with manganese complexes with linear quinol-containing ligands. With high—and physiologically unrealistic— $H_2O_2$  concentrations, catalase activity is observed. Under such conditions, quinol oxidation and the concomitant increase in  $r_1$  only occur after much of  $H_2O_2$  has been consumed.

## ASSOCIATED CONTENT

# Supporting Information

The Supporting Information is available free of charge at https://pubs.acs.org/doi/10.1021/acs.inorgchem.1c00896.

NMR, IR, UV/vis, HPLC, and MS data for  $H_4qp4$  and 1, pH titration data for  $H_4qp4$  and 1, metal-exchange data, spectroscopic and MS data for the reaction between 1 and DDQ, variable-temperature  $r_1$  measurements, and preliminary kinetic data for  $H_2O_2$  degradation (PDF)

# **Accession Codes**

CCDC 2071437 and 2071438 contain the supplementary crystallographic data for this paper. These data can be obtained free of charge via www.ccdc.cam.ac.uk/data\_request/cif, or by emailing data\_request@ccdc.cam.ac.uk, or by contacting The Cambridge Crystallographic Data Centre, 12 Union Road, Cambridge CB2 1EZ, UK; fax: +44 1223 336033.

## AUTHOR INFORMATION

## **Corresponding Author**

Christian R. Goldsmith – Department of Chemistry and Biochemistry, Auburn University, Auburn, Alabama 36849, United States; orcid.org/0000-0001-7293-1267; Email: crgoldsmith@auburn.edu

#### **Authors**

Sana Karbalaei – Department of Chemistry and Biochemistry, Auburn University, Auburn, Alabama 36849, United States

- Erik Knecht Department of Chemistry and Biochemistry, Auburn University, Auburn, Alabama 36849, United States
- Alicja Franke Department of Chemistry, Ludwig-Maximilians-Universität München, 81377 München, Germany; oorcid.org/0000-0002-6318-7429
- Achim Zahl Department of Chemistry and Pharmacy, Friedrich-Alexander University Erlangen-Nürnberg, 91058 Erlangen, Germany
- Alexander C. Saunders Department of Chemistry and Biochemistry, Auburn University, Auburn, Alabama 36849, United States
- P. Raj Pokkuluri Department of Chemistry and Biochemistry, Auburn University, Auburn, Alabama 36849, United States
- Ronald J. Beyers Magnetic Resonance Imaging Research Center, Auburn University, Auburn, Alabama 36849, United States
- Ivana Ivanović-Burmazović Department of Chemistry, Ludwig-Maximilians-Universität München, 81377 München, Germany

Complete contact information is available at: https://pubs.acs.org/10.1021/acs.inorgchem.1c00896

#### **Notes**

The authors declare no competing financial interest.

#### ACKNOWLEDGMENTS

We thank Auburn University and the National Science Foundation (Grants NSF-CHE-1662875 and NSF-CHE-1954336) for financial support.

## **■ REFERENCES**

- (1) Tretter, L.; Sipos, I.; Adam-Vizi, V. Initiation of Neuronal Damage by Complex I Deficiency and Oxidative Stress in Parkinson's Disease. *Neurochem. Res.* **2004**, *29*, 569–577.
- (2) Roberts, C. K.; Sindhu, K. K. Oxidative Stress and Metabolic Syndrome. *Life Sci.* **2009**, *84*, 705–712.
- (3) Mosley, R. L.; Benner, E. J.; Kadiu, I.; Thomas, M.; Boska, M. D.; Hasan, K.; Laurie, C.; Gendelman, H. E. Neuroinflammation, Oxidative Stress, and the Pathogenesis of Parkinson's Disease. *Clin. Neurosci. Res.* **2006**, *6*, 261–281.
- (4) Fearon, I. M.; Faux, S. P. Oxidative Stress and Cardiovascular Disease: Novel Tools Give (Free) Radical Insight. *J. Mol. Cell. Cardiol.* **2009**, *47*, 372–381.
- (5) Eskici, G.; Axelsen, P. H. Copper and Oxidative Stress in the Pathogenesis of Alzheimer's Disease. *Biochemistry* **2012**, *51*, 6289–6311.
- (6) Yu, M.; Beyers, R. J.; Gorden, J. D.; Cross, J. N.; Goldsmith, C. R. A Magnetic Resonance Imaging Contrast Agent Capable of Detecting Hydrogen Peroxide. *Inorg. Chem.* **2012**, *51*, 9153–9155.
- (7) Yu, M.; Ambrose, S. L.; Whaley, Z. L.; Fan, S.; Gorden, J. D.; Beyers, R. J.; Schwartz, D. D.; Goldsmith, C. R. A Mononuclear Manganese(II) Complex Demonstrates a Strategy to Simultaneously Image and Treat Oxidative Stress. *J. Am. Chem. Soc.* **2014**, *136*, 12836–12839.
- (8) Yu, M.; Ward, M. B.; Franke, A.; Ambrose, S. L.; Whaley, Z. L.; Bradford, T. M.; Gorden, J. D.; Beyers, R. J.; Cattley, R. C.; Ivanović-Burmazović, I.; Schwartz, D. D.; Goldsmith, C. R. Adding a Second Quinol to a Redox-Responsive MRI Contrast Agent Improves its Relaxivity Response to H<sub>2</sub>O<sub>2</sub>. *Inorg. Chem.* **2017**, *56*, 2812–2826.
- (9) Hutchinson, T. E.; Bashir, A.; Yu, M.; Beyers, R. J.; Goldsmith, C. R. An Overly Anionic Metal Coordination Environment Eliminates the *T*<sub>1</sub>-Weighted Response of Quinol-Containing MRI Contrast Agent Sensors to H<sub>2</sub>O<sub>2</sub>. *Inorg. Chim. Acta* **2019**, 496, 119045.

- (10) Wang, H.; Jordan, V. C.; Ramsay, I. A.; Sojoodi, M.; Fuchs, B. C.; Tanabe, K. K.; Caravan, P.; Gale, E. M. Molecular Magnetic Resonance Imaging Using a Redox-Active Iron Complex. *J. Am. Chem. Soc.* **2019**, *141*, 5916–5925.
- (11) Loving, G. S.; Mukherjee, S.; Caravan, P. Redox-Activated Manganese-Based MR Contrast Agent. *J. Am. Chem. Soc.* **2013**, *135*, 4620–4623.
- (12) Gale, E. M.; Mukherjee, S.; Liu, C.; Loving, G. S.; Caravan, P. Structure-Redox-Relaxivity Relationships for Redox Responsive Manganese-Based Magnetic Resonance Imaging Probes. *Inorg. Chem.* **2014**, *53*, 10748–10761.
- (13) Caravan, P.; Ellison, J. J.; McMurry, T. J.; Lauffer, R. B. Gadolinium(III) Chelates as MRI Contrast Agents: Structure, Dynamics, and Applications. *Chem. Rev.* **1999**, *99*, 2293–2352.
- (14) Drahoš, B.; Lukeš, I.; Tóth, É. Manganese(II) Complexes as Potential Contrast Agents for MRI. Eur. J. Inorg. Chem. 2012, 2012, 1975–1986.
- (15) Chen, H.; Tang, X.; Gong, X.; Chen, D.; Li, A.; Sun, C.; Lin, H.; Gao, J. Reversible Redox-Responsive <sup>1</sup>H/<sup>19</sup>F MRI Molecular Probes. *Chem. Commun.* **2020**, *56*, 4106–4109.
- (16) Hubin, T. J. Synthesis and Coordination Chemistry of Topologically Constrained Azamacrocycles. *Coord. Chem. Rev.* **2003**, 241, 27–46.
- (17) Bain, G. A.; Berry, J. F. Diamagnetic Corrections and Pascal's Constants. *J. Chem. Educ.* **2008**, *85*, 532–536.
- (18) Gans, P.; Sabatini, A.; Vacca, A. Investigation of Equilibria in Solution. Determination of Equilibrium Constants with the HYPER-QUAD Suite of Programs. *Talanta* **1996**, 43, 1739–1753.
- (19) Gale, E. M.; Žhu, J.; Caravan, P. Direct Measurement of the Mn(II) Hydration State in Metal Complexes and Metalloproteins through <sup>17</sup>O NMR Line Widths. *J. Am. Chem. Soc.* **2013**, *135*, 18600–18608
- (20) Zhang, Q.; Gorden, J. D.; Beyers, R. J.; Goldsmith, C. R. Manganese(II)-Containing MRI Contrast Agent Employing a Neutral and Non-Macrocyclic Ligand. *Inorg. Chem.* **2011**, *50*, 9365–9373.
- (21) Bernstein, M. A.; King, K. F.; Zhou, X. J. *Handbook of MRI Pulse Sequences*; Elsevier Academic Press: Amsterdam, The Netherlands, 2004.
- (22) Haacke, E. M.; Brown, R. W.; Thompson, M. R.; Venkatesan, R. Magnetic Resonance Imaging: Physical Principles and Sequence Design; John Wiley & Sons: New York, 1999.
- (23) Nelder, J. A.; Mead, R. A Simplex Method for Function Minimization. *Comput. J.* **1965**, *7*, 308–313.
- (24) Nelson, D. P.; Kiesow, L. A. Enthalpy of Decomposition of Hydrogen Peroxide by Catalase at  $25^{\circ}$  C (with Molar Extinction Coefficients of  $H_2O_2$  Solutions in the UV). *Anal. Biochem.* **1972**, 49, 474–478.
- (25) Luo, H.; Rogers, R. D.; Brechbiel, M. A Convenient and Selective Route to a *trans*-Difunctionalized Macrocyclic Hexadentate  $N_4O_2$  Ligand. *Can. J. Chem.* **2001**, *79*, 1105–1109.
- (26) Goldsmith, C. R.; Cole, A. P.; Stack, T. D. P. C-H Activation by a Mononuclear Manganese(III) Hydroxide Complex: Synthesis and Characterization of a Manganese-Lipoxygenase Mimic? *J. Am. Chem. Soc.* 2005, 127, 9904–9912.
- (27) Coates, C. M.; Nelson, A.-G. D.; Goldsmith, C. R. The Influence of Ligand Electronics on the Metrical Parameters and Redox Potentials of a Series of Manganese(II) Compounds. *Inorg. Chim. Acta* **2009**, 362, 4797–4803.
- (28) Klein Gebbink, R. J. M.; Jonas, R. T.; Goldsmith, C. R.; Stack, T. D. P. A Periodic Walk: A Series of First-Row Transition Metal Complexes with the Pentadentate Ligand PY5. *Inorg. Chem.* **2002**, *41*, 4633–4641.
- (29) Shongwe, M. S.; Mikuriya, M.; Ainscough, E. W.; Brodie, A. M. Molecular Structure of  $[MnL_2]-[H_2L=N-(3,5-Dichloro-2-hydroxybenzyl)$ glycine]: Evidence for a Pseudo-Jahn–Teller Compression. *J. Chem. Soc., Chem. Commun.* **1994**, 887–888.
- (30) Motekaitis, R. J.; Rogers, B. E.; Reichert, D. E.; Martell, A. E.; Welch, M. J. Stability and Structure of Activated Macrocycles. Ligands with Biological Applications. *Inorg. Chem.* **1996**, *35*, 3821–3827.

- (31) Sahoo, S. C.; Dubey, M.; Alam, M. A.; Ray, M. Effect of Metal Coordination and Intra-Molecular H-Bond on the Acidity of Phenolic Proton in a Set of Structurally Characterized Octahedral Ni(II) Complexes of L-Histidine Derivative. *Inorg. Chim. Acta* **2010**, 363, 3055–3060.
- (32) Ward, M. B.; Scheitler, A.; Yu, M.; Senft, L.; Zillmann, A. S.; Gorden, J. D.; Schwartz, D. D.; Ivanović-Burmazović, I.; Goldsmith, C. R. Superoxide Dismutase Activity Enabled by a Redox-Active Ligand rather than a Metal. *Nat. Chem.* **2018**, *10*, 1207–1212.
- (33) Senft, L.; Moore, J. L.; Franke, A.; Fisher, K. R.; Scheitler, A.; Zahl, A.; Puchta, R.; Fehn, D.; Ison, S.; Sader, S.; Ivanović-Burmazović, I.; Goldsmith, C. R. Quinol-Containing Ligands Enable High Superoxide Dismutase Activity by Modulating Coordination Number, Charge, Oxidation States and Stability of Manganese Complexes throughout Redox Cycling. Unpublished work.
- (34) Dees, A.; Zahl, A.; Puchta, R.; van Eikema Hommes, N. J. R.; Heinemann, F. W.; Ivanović-Burmazović, I. Water Exchange on Seven-Coordinate Mn(II) Complexes with Macrocyclic Pentadentate Ligands: Insight in the Mechanism of Mn(II) SOD Mimetics. *Inorg. Chem.* **2007**, *46*, 2459–2470.
- (35) Kenkel, I.; Franke, A.; Dürr, M.; Zahl, A.; Dücker-Benfer, C.; Langer, J.; Filipović, M. R.; Yu, M.; Puchta, R.; Fiedler, S. R.; Shores, M. P.; Goldsmith, C. R.; Ivanović-Burmazović, I. Switching between Inner- and Outer-Sphere PCET Mechanisms of Small Molecule Activation: Superoxide Dismutation and Oxygen/Superoxide Reduction Reactivity Deriving from the Same Manganese Complex. *J. Am. Chem. Soc.* 2017, 139, 1472–1484.
- (36) Lieb, D.; Friedel, F. C.; Yawer, M.; Zahl, A.; Khusniyarov, M. M.; Heinemann, F. W.; Ivanović-Burmazović, I. Dinuclear Seven-Coordinate Mn(II) Complexes: Effect of Manganese(II)-Hydroxo Species on Water Exchange and Superoxide Dismutase Activity. *Inorg. Chem.* **2013**, *52*, 222–236.
- (37) Gale, E. M.; Atanasova, I. P.; Blasi, F.; Ay, I.; Caravan, P. A Manganese Alternative to Gadolinium for MRI Contrast. *J. Am. Chem. Soc.* **2015**, *137*, 15548–15557.
- (38) Troughton, J. S.; Greenfield, M. T.; Greenwood, J. M.; Dumas, S.; Wiethoff, A. J.; Wang, J.; Spiller, M.; McMurry, T. J.; Caravan, P. Synthesis and Evaluation of a High Relaxivity Manganese(II)-Based MRI Contrast Agent. *Inorg. Chem.* **2004**, *43*, 6313–6323.
- (39) Molnár, E.; Camus, N.; Patinec, V.; Rolla, G. A.; Botta, M.; Tircsó, G.; Kálmán, F. K.; Fodor, T.; Tripier, R.; Platas-Iglesias, C. Picolinate-Containing Macrocyclic Mn<sup>2+</sup> Complexes as Potential MRI Contrast Agents. *Inorg. Chem.* **2014**, *53*, 5136–5149.
- (40) Botár, R.; Molnár, E.; Trencsényi, G.; Kiss, J.; Kálmán, F. K.; Tircsó, G. Stable and Inert Mn(II)-Based and pH-Responsive Contrast Agents. J. Am. Chem. Soc. 2020, 142, 1662–1666.
- (41) McGowan, P. C.; Podesta, T. J.; Thornton-Pett, M. N-Monofunctionalized 1,4,7-Triazacyclononane Macrocycles as Building Blocks in Inorganic Crystal Engineering. *Inorg. Chem.* **2001**, 40, 1445–1453.
- (42) Major, J. L.; Parigi, G.; Luchinat, C.; Meade, T. J. The Synthesis and in Vitro Testing of a Zinc-Activated MRI Contrast Agent. *Proc. Natl. Acad. Sci. U. S. A.* **2007**, *104*, 13881–13886.
- (43) Regueiro-Figueroa, M.; Rolla, G. A.; Esteban-Gómez, D.; de Blas, A.; Rodríguez-Blas, T.; Botta, M.; Platas-Iglesias, C. High Relaxivity Mn<sup>2+</sup>-Based MRI Contrast Agents. *Chem. Eur. J.* **2014**, *20*, 17300–17305.
- (44) Wang, S.; Westmoreland, T. D. Correlation of Relaxivity with Coordination Number in Six-, Seven-, and Eight-Coordinate Mn(II) Complexes of Pendant-Arm Cyclen Derivatives. *Inorg. Chem.* **2009**, 48, 719–727.
- (45) Phukan, B.; Mukherjee, C.; Goswami, U.; Sarmah, A.; Mukherjee, S.; Sahoo, S. K.; Moi, S. C. A New Bis(aquated) High Relaxivity Mn(II) Complex as an Alternative to Gd(III)-Based MRI Contrast Agent. *Inorg. Chem.* **2018**, *57*, 2631–2638.
- (46) Gale, E. M.; Jones, C. M.; Ramsay, I.; Farrar, C. T.; Caravan, P. A Janus Chelator Enables Biochemically Responsive MRI Contrast with Exceptional Dynamic Range. *J. Am. Chem. Soc.* **2016**, *138*, 15861–15864.

- (47) Geraldes, C. F. G. C.; Sherry, A. D.; Brown, R. D., III; Koenig, S. H. Magnetic Field Dependence of Solvent Proton Relaxation Rates Induced by Gd<sup>3+</sup> and Mn<sup>2+</sup> Complexes of Various Polyaza Macrocyclic Ligands: Implications for NMR Imaging. *Magn. Reson. Med.* **1986**, 3, 242–250.
- (48) Chaves, S.; Delgado, R.; Da Silva, J. J. R. F. The Stability of the Metal Complexes of Cyclic Tetra-aza Tetra-acetic Acids. *Talanta* **1992**, 39, 249–254.
- (49) Aime, S.; Baroni, S.; Delli Castelli, D.; Brücher, E.; Fábián, I.; Serra, S. C.; Fringuello Mingo, A.; Napolitano, R.; Lattuada, L.; Tedoldi, F.; Baranyai, Z. Exploiting the Proton Exchange as an Additional Route to Enhance the Relaxivity of Paramagnetic MRI Contrast Agents. *Inorg. Chem.* **2018**, *57*, 5567–5574.
- (50) Kinnula, V. L.; Everitt, J. I.; Whorton, A. R.; Crapo, J. D. Hydrogen Peroxide Production by Alveolar Type II Cells, Alveolar Macrophages, and Endothelial Cells. *Am. J. Physiol.* **1991**, *261*, L84–91.
- (51) Lyublinskaya, O.; Antunes, F. Measuring Intracellular Concentration of Hydrogen Peroxide with the Use of Genetically Encoded H<sub>2</sub>O<sub>2</sub> Biosensor HyPer. *Redox Biol.* **2019**, *24*, 101200.
- (52) Sies, H. Role of Metabolic H<sub>2</sub>O<sub>2</sub> Generation REDOX SIGNALING AND OXIDATIVE STRESS. J. Biol. Chem. **2014**, 289, 8735–8741.